Optical Properties of Aerosol Particles over the Northeast Pacific

JULIA MARSHALL,* ULRIKE LOHMANN,*,+ W. RICHARD LEAITCH,# NICOLE SHANTZ,@ LISA PHINNEY,* DESIREE TOOM-SAUNTRY,# AND SANGEETA SHARMA#

*Department of Physics and Atmospheric Science, Dalhousie University, Halifax, Nova Scotia, Canada
+ETH Institute for Atmospheric and Climate Science, Zurich, Switzerland
#Meteorological Service of Canada, Environment Canada, Downsview, Ontario, Canada
@Centre for Research in Earth and Space Sciences, York University, Toronto, Ontario, Canada

(Manuscript received 4 May 2004, in final form 4 February 2005)

ABSTRACT

In July 2002, atmospheric aerosol measurements were conducted over the northeast Pacific Ocean as part of the Subarctic Ecosystem Response to Iron Enhancement Study (SERIES). The following aerosol quantities were measured: particle number size distribution, particle scattering and backscattering coefficients at three wavelengths, particle absorption coefficient at one wavelength, and size-segregated particle chemical composition. Using Mie theory to calculate the aerosol particle scattering and absorption coefficients from the size distribution and chemical measurements, closure with the measured optical coefficients is not attained. Discrepancies between the calculated and measured scattering and backscattering coefficients are largely a result of the fact that the nephelometer measures scattering only between 7° and 170°. Over 90% of the total scattering and 50% of the backscattering in this study was not measured by the nephelometer because of the missing forward-scattering (0°–7°) and backscattering (170°–180°) segments of the phase function. During this study the majority of the total scattering and backscattering in the marine boundary layer of this region was a result of coarse particles consisting almost entirely of sea salt.

1. Introduction

Aerosol particles can influence the earth's radiative budget through scattering and absorption of both incoming and outgoing radiation (Seinfeld and Pandis 1998). Aerosols may scatter incoming shortwave radiation back to space, cooling the atmosphere. Some aerosols, such as black carbon, absorb the shortwave solar radiation and consequently warm the atmosphere. These processes are the direct effect of aerosols on climate.

The total extinction coefficient (σ_{ext}) is determined by absorption and scattering by both gas molecules and aerosol particles, as given by Eq. (1):

$$\sigma_{ext} = \sigma_{sp} + \sigma_{ap} + \sigma_{sg} + \sigma_{ag}, \quad (1)$$

where σ_{sp} is the scattering coefficient by aerosol particles, integrated between 0° and 180°, and σ_{ap} is the absorption coefficient resulting from aerosol particles; σ_{sg} and σ_{ag} are the same quantities, but result from the effects of gas molecules.

The backscattering coefficient resulting from aerosol particles (σ_{bsp}) is the same as the scattering coefficient, only integrated between 90° and 180° (Carrico et al. 1998).

The direct aerosol effect is determined by the optical properties of the aerosol particles, which are dependent upon the size, shape, and composition of the particles and the wavelength of the incident light. Measurements of the aerosol optical properties through the use of an integrating nephelometer or a particle soot absorption photometer (PSAP) are unable to apportion these effects into the contributions from individual chemical species (Anderson et al. 1999).

In a closure experiment an aerosol property is measured in one or more ways, and then calculated from a model based upon independently measured data (e.g., Quinn and Coffman 1998). The comparison between the calculated and measured values is a basis for the level of confidence in both the measurements and the model. To perform an optical closure study, it is necessary to know the chemical composition of the aerosols, their complex refractive indices, their size distri-

Corresponding author address: Julia Marshall, Canadian Centre for Climate Modelling and Analysis, University of Victoria, P.O. Box 1700, STN CSC, Victoria, BC V8W 2Y2, Canada.
E-mail: marshall@mathstat.dal.ca

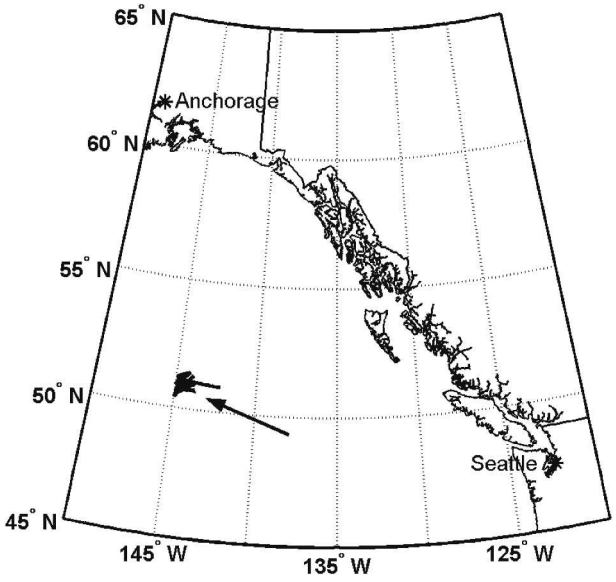

FIG. 1. The region of the ocean where the study took place, off the west coast of Canada. The path of the ship is plotted as a solid line, indicated with the arrow.

butions, and their observed optical properties (i.e., scattering, backscattering, and absorption coefficients).

Such an optical closure study is performed here by comparing the measured aerosol particle scattering and absorption coefficients with those calculated from Mie theory using the measurements of the aerosol particle size distribution and the size-resolved chemical constituents as inputs to the model.

This study provides optical data for the remote environment of the northeast Pacific Ocean, in the region of 50.37°–51.41°N, 142.23°–145.00°W. The path of the ship during the sampling period is shown in Fig. 1. According to assessments of single scattering albedo measurements (Liousse et al. 1996; Heintzenberg et al. 1997), this is part of a region with notably scarce data.

2. Measurements

The data were collected as part of the Subarctic Ecosystem Response to Iron Enrichment Study (SERIES), an experiment of the Canadian Surface Ocean–Lower Atmosphere Study (C-SOLAS) program. The platform was the Mexican research vessel *El Puma*, which left from Sidney, British Columbia, Canada, on 2 July 2002, for the study region of approximately 1400 km into the northeastern Pacific. The data were collected over the course of the cruise, from 5 to 30 July 2002. In this paper, only the data collected from 20 to 30 July will be considered, because of the full functionality of the instruments over that time period.

The measurements relevant to this study are the size spectra of the aerosols, their chemical constituents, and the scattering and absorption coefficients of the aerosols. The inlets for all the measurements involved were located at approximately 12 m above sea level.

The size spectra were measured with a TSI Scanning Mobility Particle Sampler (SMPS), a Particle Measuring Systems, Inc. (PMS), Passive Cavity Aerosol Spectrometer Probe (PCASP), and a PMS Forward Scattering Spectrometer Probe (FSSP). These instruments have size ranges of 0.008–0.32, 0.15–3.0, and 2.0–47.0 μm, respectively. The inorganic chemical data used here were collected with a 10-stage multiple orifice uniform distribution impactor (MOUDI), with midpoint diameters ranging from 0.06 to 18 μm. The MOUDI was used in a static, as opposed to a rotating, mode. The scattering and backscattering coefficients were measured with a TSI 3563 Integrating Nephelometer, and the absorption coefficient was measured with a PSAP. The nephelometer measures scattering and backscattering coefficients at three different wavelengths (blue, 0.45 μm; green, 0.55 μm; and red, 0.70 μm), while the PSAP measures the absorption coefficient for green light only. Last, the concentration of SO_2 was measured by a pulsed fluorescent ambient SO_2 analyzer in order to detect the presence of ship exhaust in the samples. These instruments are summarized in Table 1.

All of the data were interpolated to a 10-min time step, with the exception of the MOUDI filter data that were integrated over sampling periods ranging from 6 to 16 h (mean of approximately 9 h). Other than the MOUDI data, all of the data were filtered to remove the presence of ship exhaust in the data. To determine when ship exhaust was present measurements of SO_2 were employed, because it is a by-product of the combustion of sulfur-containing fuels. The SO_2 levels were measured every minute. Whenever the concentration of SO_2 rose above 1 ppb, the data were considered to be tainted by ship exhaust and were removed from the study.

The MOUDI filters were only employed when the air was considered to be free from exhaust. Ten sets of clean MOUDI data were collected over the time period in question, and three blanks.

The averaged data for the MOUDI filters is shown in Fig. 2. The composition of the aerosol as a function of diameter is a necessary input to the Mie calculations in order to carry out the optical closure study. The MOUDI analysis separates the inorganic constituents into the following categories: Cl^-, NO_2^-, Br^-, NO_3^-, $SO_4^=$, $C_2O_4^=$, Na^+, NH_4^+, K^+, Mg^{++}, Ca^{++}, MSA. For the purposes of this study, these were grouped into $(Na^+ + Cl)$, $(NO_2^- + NO_3^-)$, $(NH_4^+ + SO_4^=)$, MSA, and other, based upon Li et al. (1998). The coarse-particle mass was dominated by $(Na^+ + Cl^-)$, whereas the fine-

TABLE 1. A summary of the instruments used, the size range over which they operate and a description of their function.

Instrument	Size range	Description
SMPS	0.008–0.320 μm, with 26 size bins	Charges particles and sizes them based on their mobility within an electric field
PCASP	0.15–3.0 μm, with 15 size bins	An intrusive optical particle counter (OPC) that sizes particles based on the amount of light each one scatters
FSSP	2.0–47.0 μm, with 15 size bins	A nonintrusive OPC, using the forward-scattered light from an incident laser to determine the size of larger particles
MOUDI	0.03–18.0, μm in 12 stages	A 12-stage impactor using Teflon filters as the collection surface at each stage; particles collected on each filter are subsequently analyzed by ion chromatography
AMS	0.06–0.6-μm vacuum aerodynamic diameter at 100% efficiency; efficiency drops outside this size range (Zhang et al. 2002)	Aerosols are sized by vacuum time-of-flight measurements then vaporized, ionized, and passed through a mass spectrometer; this determines the size distribution and mass concentration of nonrefractive aerosol species
PSAP	$>$0.01 μm	Absorption is based on the attenuation of green light (0.565 μm) by the particles collected on a filter
Integrating nephelometer	$>$95% of particles with an aerodynamic diameter from 0.05 to 5.0 μm, with collection efficiency falling after that	Measurement of the light scattered by a defined volume of particles at three wavelengths (0.45, 0.55, and 0.70 μm)
Pulsed fluorescent ambient SO_2 analyzer	—	Pulsating ultraviolet light is focused into a fluorescence chamber filled with sample air, thereby exciting SO_2 molecules into higher energy states; these molecules then emit a characteristic radiation as these energy states decay; this radiation is filtered and measured by a photomultiplier tube

particle mass was predominantly ($NH_4^+ + SO_4^=$). The submicron sulfate results agree well with the measurements from an Aerodyne Aerosol Mass Spectrometer (AMS), as demonstrated by Phinney et al. (2004, manuscript submitted to *Deep-Sea Res.*). No comparison could be made for the levels of ($Na^+ + Cl^-$) because the AMS evaporator does not operate at a sufficiently high temperature to volatilize sea salt. Though the AMS inorganic data were measured at a higher time resolution than the MOUDI data, they are not used in this study because of the inability of the AMS to measure supermicron aerosols and sea salt.

The AMS is able to measure the organic fraction of the aerosol, though it provides little information on the individual species. This makes it difficult to estimate the optical properties of the organics. Because the organic concentration is relatively low during the period of interest, as shown in Fig. 3, and because their optical properties are not known, the organic fraction is not included in the calculations. Including the organics and assuming that they have the same optical properties as sulfate changes the results by less than 4% throughout. The complex indices of refraction for ammonium sulfate and sea salt (Tang 1996; Toon et al. 1976) are used as inputs to the calculations.

Figure 4 shows both the number concentration and surface area averaged over the period in which the data are being analyzed. Though the number concentration peak is firmly in the submicron range, the surface area peak is in the coarse mode, which is often typical for marine aerosols (Seinfeld and Pandis 1998).

The scattering coefficients that are measured with the nephelometer are shown in Fig. 5. The blue wavelength has the highest scattering and backscattering coefficient, followed by the green and the red. This is consistent with Mie theory, which indicates that particles of sizes that are smaller than or comparable to the wavelength of light exhibit a preference to scatter smaller wavelengths (Bohren and Huffman 1998).

The cruise averages of the scattering coefficients are 20 ± 14, 17 ± 13, and 14 ± 11 Mm^{-1} for blue, green, and red light, respectively. For the backscattering coefficients the averages are 2.1 ± 1.6, 1.9 ± 1.3, and 1.6 ± 1.1 Mm^{-1}. The $\pm$ value represents one standard deviation from the mean. The measurement uncertainty is less than 0.2 Mm^{-1} in all cases.

3. Analysis

a. Mie calculations

The optical model used here is an adaptation of the Mie code outlined in Bohren and Huffman (1998), integrating over specific angular contributions so as to account for the angular truncation of the nephelometer. All of the chemical constituents are assumed to be ex-

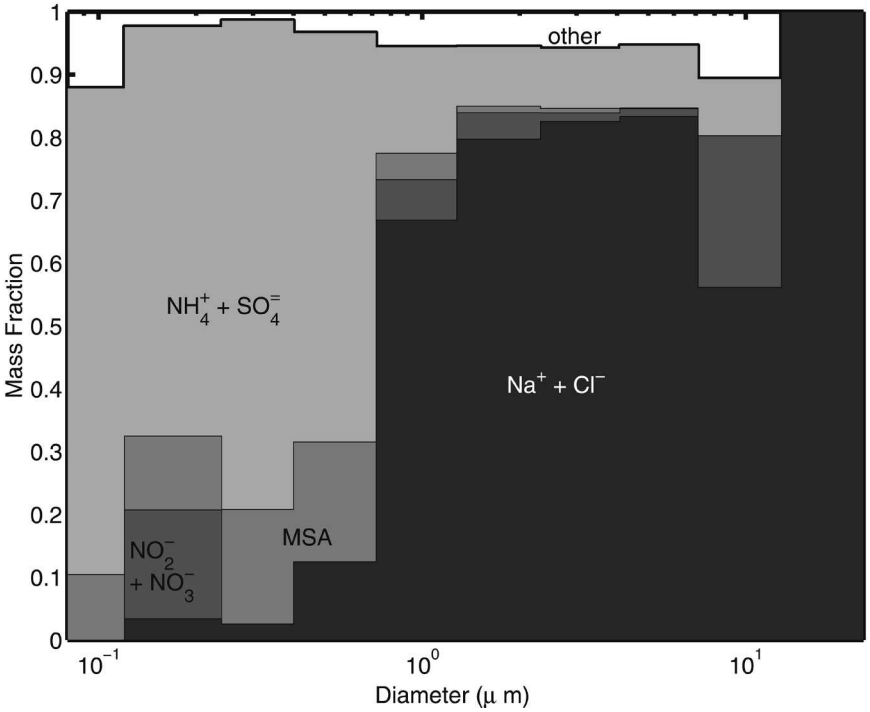

FIG. 2. The average fractional concentration of chemical constituents as measured by the MOUDI filters.

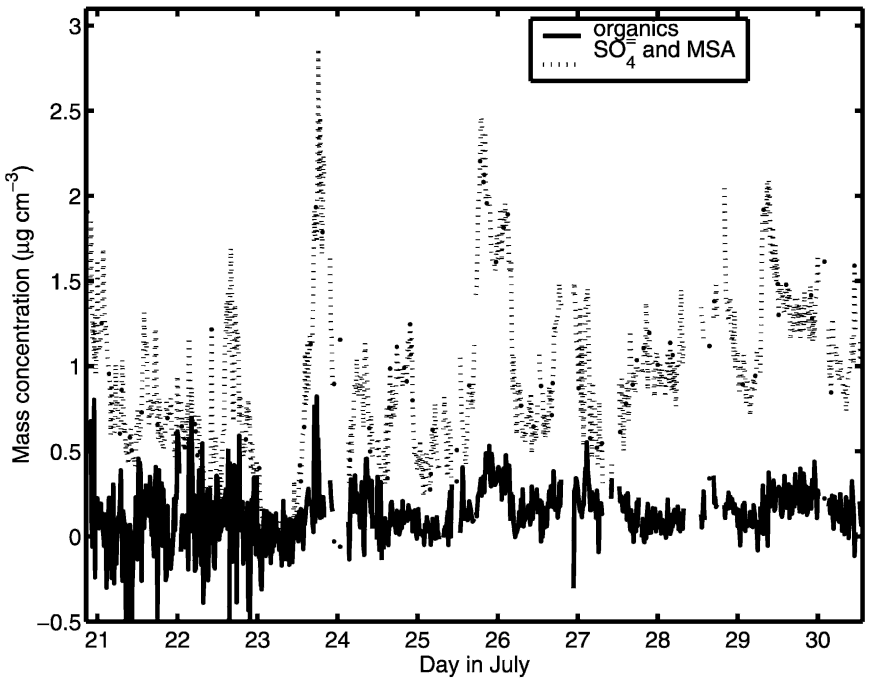

FIG. 3. The mass concentration of organics and sulfur species ($SO_4^=$ and MSA) as measured by the AMS. Over the time period sampled the organic fraction of the aerosol represented only a small fraction of the mass as compared with the sulfur species.

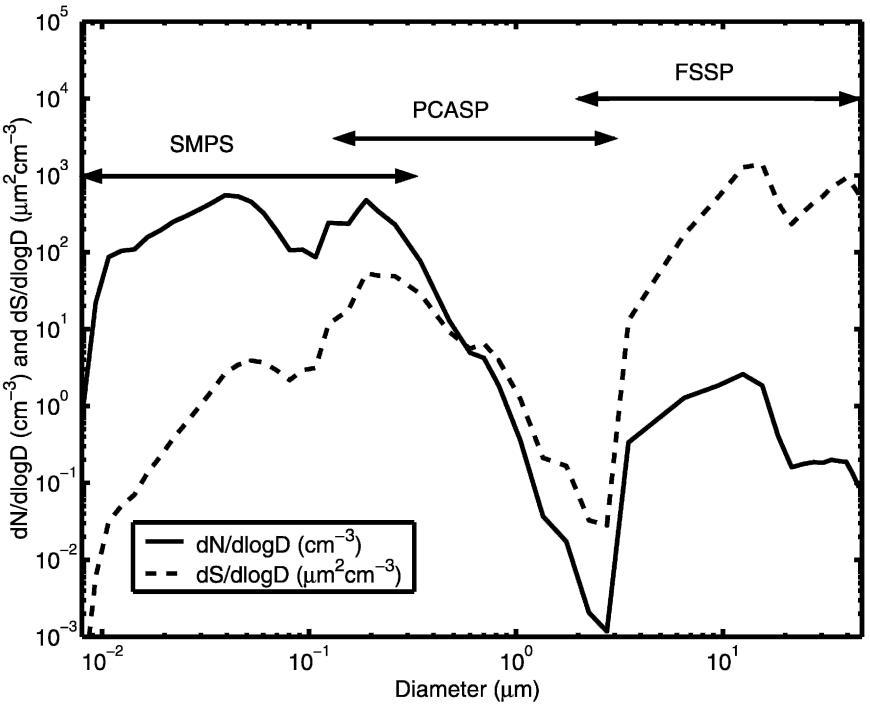

FIG. 4. Lognormal number (solid line) and surface area (dashed line) concentrations as a function of diameter. The sampling range of each instrument (SMPS, PCASP, and FSSP) is indicated.

ternally mixed. This assumption should not greatly affect the results, because of the dominance of NaCl or $NH_4^+ + SO_4^=$ (Li et al. 1998; Tang 1997) and the scarcity of black carbon.

The inputs for the Mie calculations were the time series of the aerosol size spectra, and the time series of the size-segregated chemical constituents as measured by the MOUDI filters. The time step of these two sets of data is very different, but the MOUDI values were assumed to be constant over each sampling period until the next sampling period began, while the size spectra changed every 10 min. The Mie calculations were carried out for each 10-min time step.

The calculated and measured scattering coefficients for the green wavelength are shown in Fig. 6. Similar results are found for red and blue light. When compared with the value calculated using Mie theory, the nephelometer signal is smaller by more than an order of magnitude throughout most of the time series. This is largely a result of the angular truncation in the measurement; because of the geometry of the nephelometer, scattering is only measured between 7° and 170°. Much better agreement was attained by incorporating this angular limitation into the Mie calculations. With this limitation accounted for, the measurable theoretical curve agrees fairly well, and the two are usually within about 15% of each other, as shown in Fig. 7. The times when this ceases to be true are the evenings of 21 and 23 July, when the measured scattering was exceptionally high.

This is a well-recognized limitation of the nephelometer (Anderson et al. 1996), and is discussed at length by Anderson and Ogren (1998). Their suggested correction factor for the total scattering coefficient for sampling without a size cut ($\lambda = 0.55\ \mu$m) of 1.29 ± 0.23 is much smaller than the correction factor that is necessary in this case.

The disagreement between the measured signal and the theoretical signal can be largely attributed to the dominant forward-scattering signal of the coarse aerosol particles. The phase function for larger scatterers is concentrated in one large central lobe, which is largely missed when neglecting the contribution between 0° and 7°. This can be seen in a diagram of phase functions, found in Fig. 8. Here the region that cannot be measured by the nephelometer is demarcated with solid lines. Clearly, for large scatterers, relatively little of the signal can be measured.

To examine the measurable backscattering, the effects of the forward and backward angular truncations were separated. Figure 9 shows the calculated σ_{bspc} (from 90° to 180°) as a function of scatterer diameter,

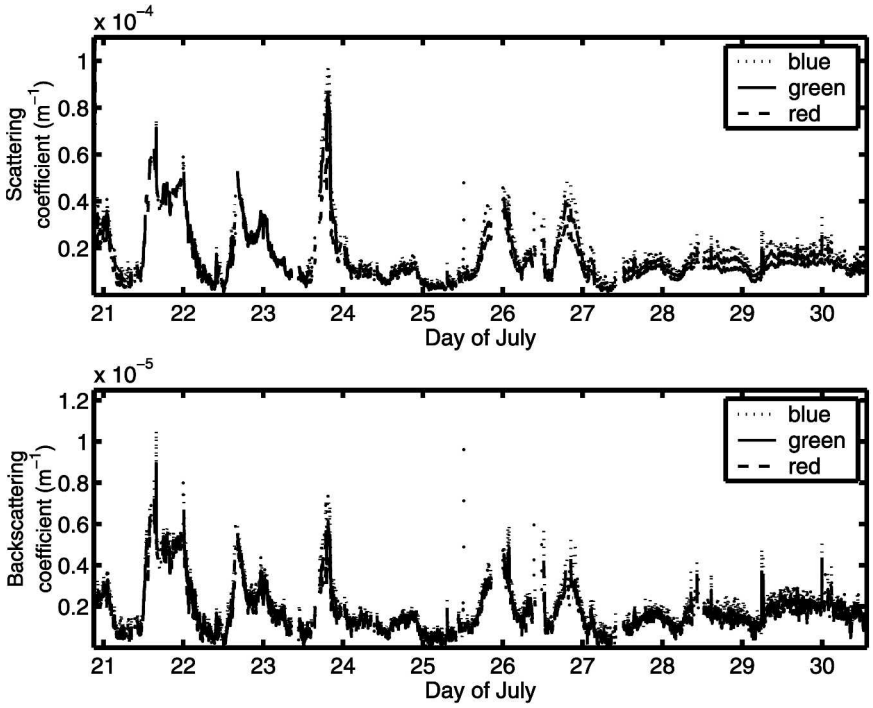

FIG. 5. (a) The top three curves represent the scattering coefficients (σ_{sp}) for three different wavelengths of light as measured by the integrating nephelometer at 0.45 (dotted line), 0.55 (solid line), and 0.70 (dashed line) μm. For much of the plot the signals at 0.55 and 0.70 μm are difficult to distinguish from one another, but the signal at 0.55 μm is greater than that at 0.70 μm. (b) The same information, but for backscattering coefficients (σ_{bsp}).

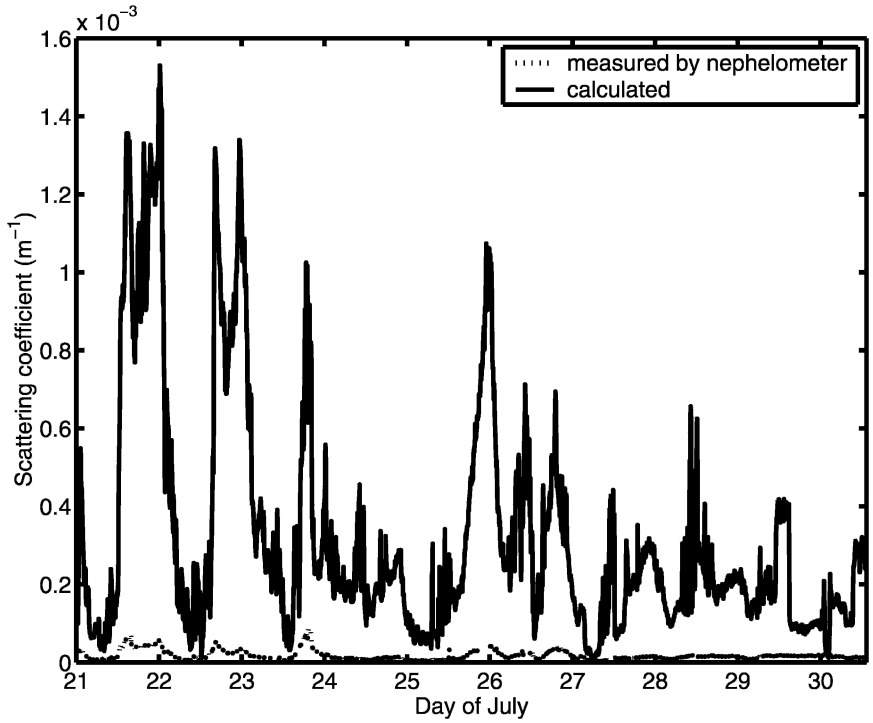

FIG. 6. The dotted line shows the measured scattering coefficient (σ_{sp}) for green light, while the solid line shows the calculated value (σ_{spc}) based upon the size spectra and the chemical information.

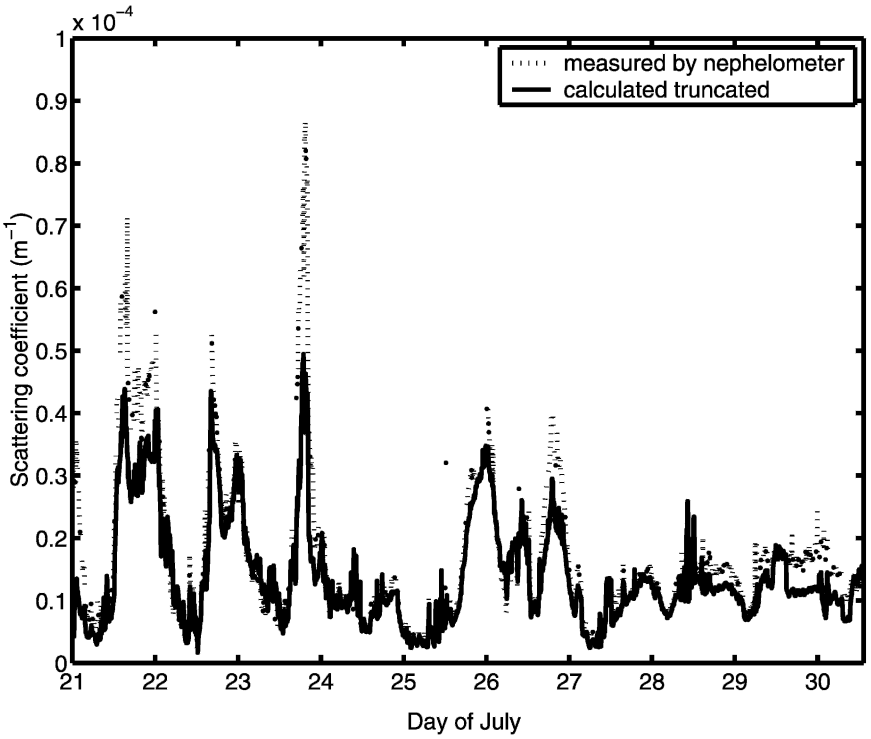

FIG. 7. The measured scattering coefficient by aerosol particles (σ_{sp}) is shown in the dotted line, and the calculated truncated value, based upon the angular limitations of the nephelometer (σ_{spt}), is plotted as the solid line.

along with the calculated truncated value σ_{bspt}, resulting from the backward truncation between 170° and 180°. Not only is the angular truncation significant, but about half of the signal is missed for scatterers larger than 1 μm.

Applying these results to the measured data yields Fig. 10. Again, the calculated value from Mie theory is much larger than that measured by the nephelometer. However, when the angular correction is applied the agreement is even better than for the total scattering, with no systematic underestimation. Similar results were found when the analysis was repeated for the other two wavelengths. The findings are summarized in Table 2.

The absorption coefficient measured by the PSAP was corrected for flow, spot size, and uncertainties in the instrument, as outlined in Bond et al. (1999). After these corrections the mean absorption coefficient (σ_{ap}) measured with the PSAP was 1.3 ± 0.6 Mm^{-1}, with the uncertainty derived from the correction factors in Bond et al. (1999). The calculated value, based only on the absorption by the inorganic species, is 1.3 ± 0.9 Mm^{-1}. These values are in excellent agreement and indicate that black carbon was not a significant factor in this particular environment.

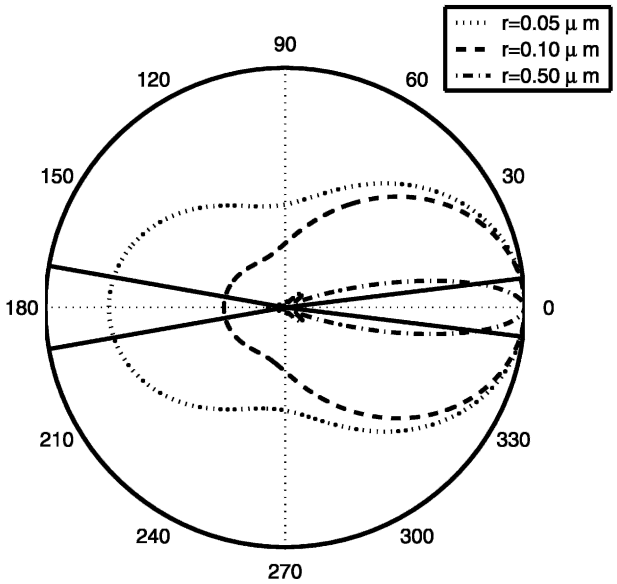

FIG. 8. Scattering phase functions for a variety of particle radii. All calculations here assumed that $\lambda = 0.55$ μm, and $m = 1.55 + 0i$, representing SiO_2. The phase functions are normalized in the forward-scattering direction for ease of display. The regions delineated in the solid line cannot be measured by the nephelometer.

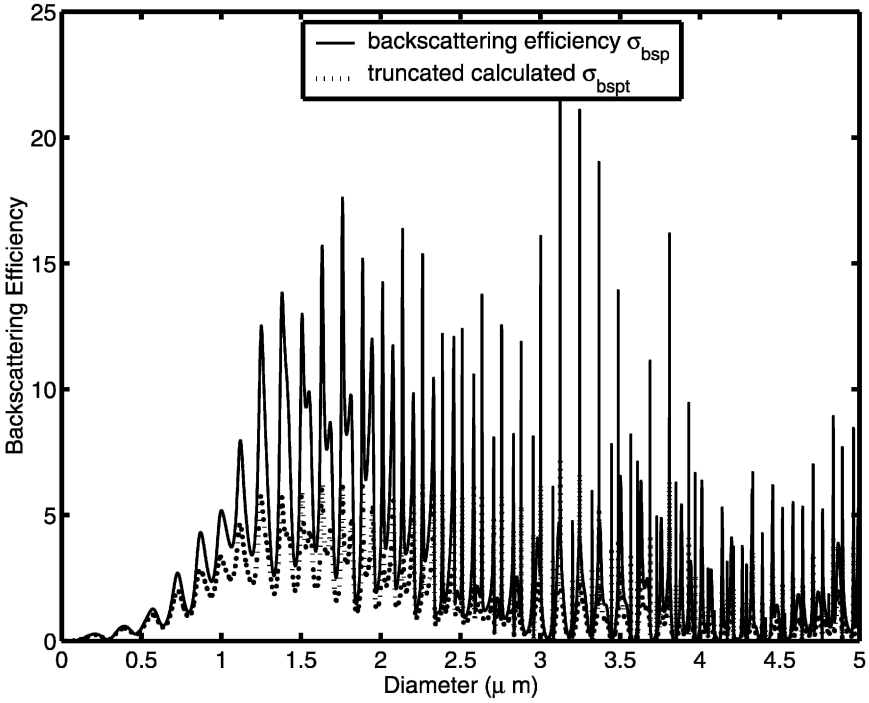

FIG. 9. The backscatter coefficient for particles σ_{bsp} as a function of scatterer diameter (solid), and the calculated truncated backscattering coefficient σ_{bspt} resulting from angular truncations (dotted).

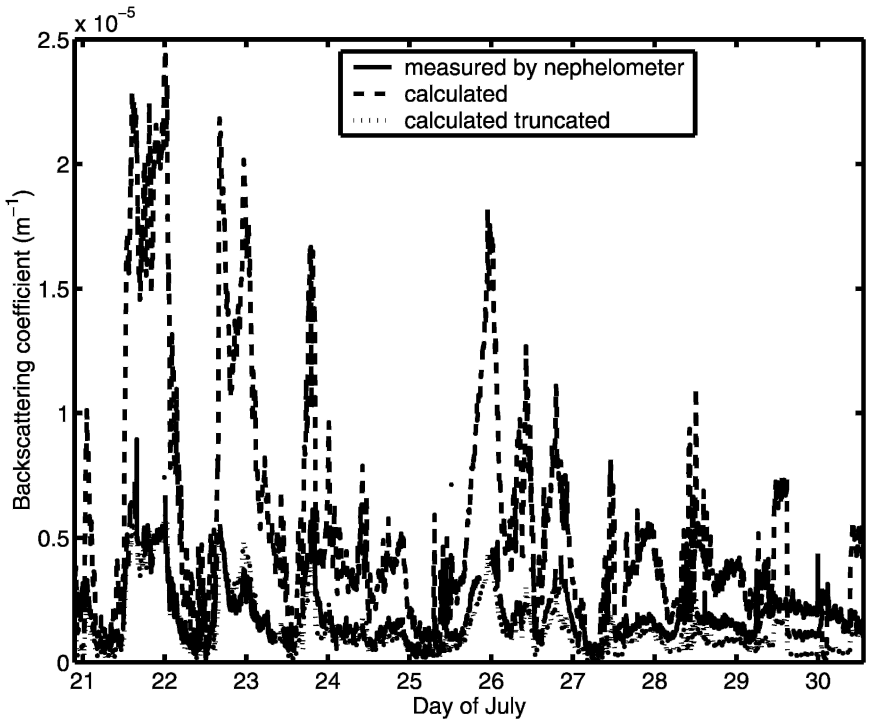

FIG. 10. The measured value of σ_{bsp} for green light (solid line), the calculated value (via Mie theory based upon size and chemical information) σ_{bspc} (dashed line), and the calculated truncated value σ_{bspt} (dotted line) are shown.

TABLE 2. A summary of the scattering and backscattering coefficients; measured, calculated, and calculated truncated values for all three wavelengths. The given errors are one standard deviation of the mean, and in all cases are higher than the uncertainties resulting from instrumentation.

	Total scattering coefficients			Backscattering coefficients		
λ (μm)	Measured σ_{sp} (Mm^{-1})	Calculated σ_{spc} (Mm^{-1})	Truncated σ_{spt} (Mm^{-1})	Measured σ_{bsp} (Mm^{-1})	Calculated σ_{bspc} (Mm^{-1})	Truncated σ_{bspt} (Mm^{-1})
0.45	20 ± 14	320 ± 290	15 ± 6	2.1 ± 1.6	5.4 ± 5.0	2.4 ± 2.1
0.55	17 ± 13	320 ± 300	13 ± 7	1.9 ± 1.3	4.7 ± 4.6	2.0 ± 1.9
0.70	14 ± 11	320 ± 300	12 ± 10	1.6 ± 1.1	2.7 ± 2.6	1.4 ± 1.4

Given the scattering and absorption coefficients, one can estimate the aerosol optical depth τ of the marine boundary layer, using Eq. (2):

$$\tau = \sigma_{ext} z = (\sigma_{ap} + \sigma_{sp}) z, \quad (2)$$

where z is the estimated depth of the well-mixed boundary layer (Seinfeld and Pandis 1998). If we use the calculated values of σ_{spc} and σ_{apc}, and assume a boundary layer of 300 m, this yields a τ of approximately 0.1 at 0.55 μm. This compares well with the findings of Smirnov et al. (1995), which give a τ of 0.09–0.12 for air over the Pacific with similar synoptic conditions, though integrated over the whole atmosphere. The implication of the agreement is that sea salt in the marine boundary layer may often dominate the aerosol optical depth of the troposphere over the North Pacific.

b. Attribution of scattering by size

There was no separate sampling of submicron and supermicron aerosols with the nephelometer, so it is necessary to analyze the data after the fact to attempt to apportion the scattering based upon size. The contribution of each size bin to the scattering is shown in Fig. 11. These data are based purely upon the calculated results from the measured size spectra and chemical information.

The calculated scattering coefficient (σ_{spc}) indicates

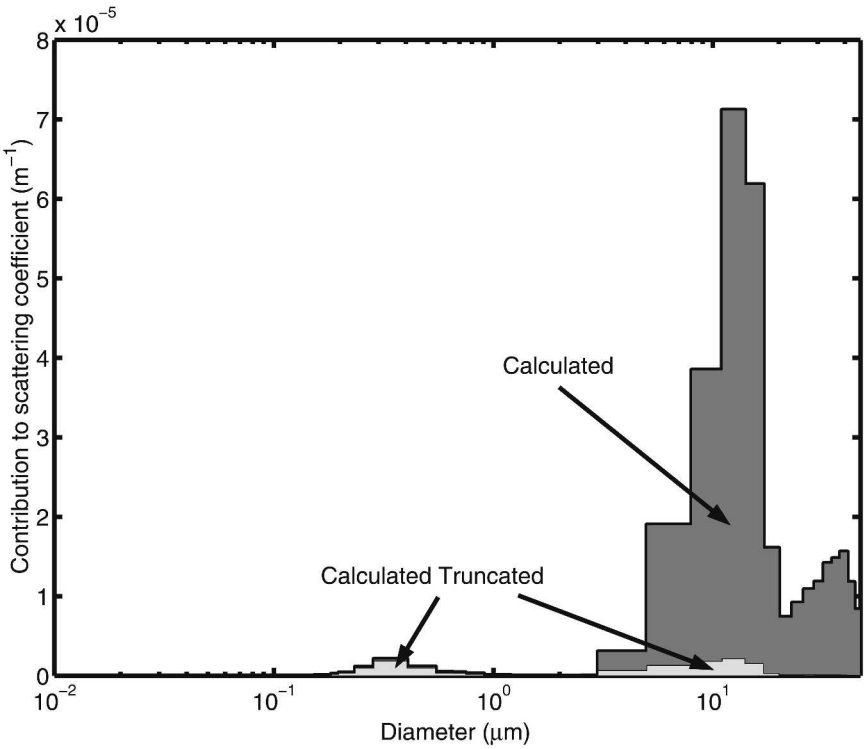

FIG. 11. The calculated scattering coefficient σ_{spc} (dark gray) and the truncated calculated scattering coefficient σ_{spt} (light gray), both as a function of diameter.

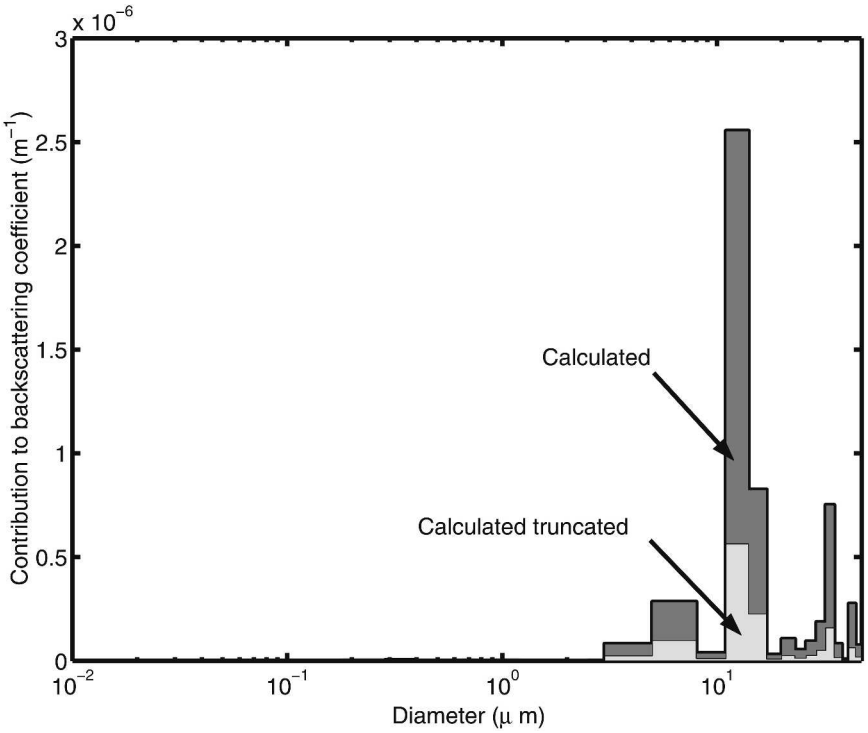

FIG. 12. The calculated backscattering coefficient σ_{bspc} as a function of diameter (dark gray), and the same calculation including angular truncation σ_{bspt} (light gray).

that the vast majority of the scattering is a result of particles in the coarse mode, particularly around 10 μm. The values calculated when considering the angular truncation are much lower in the coarse mode, whereas the contribution to scattering from the fine mode changes relatively little. The truncated calculated scattering coefficient (σ_{spt}) is more evenly distributed between the two modes.

The same analysis was carried out for the backscattering coefficients, and is shown in Fig. 12. Again, most of the backscattering is from the coarse particles because of their dominance during the cruise. The fine mode is even less evident than in the case of total scattering. The gap between the calculated value and the calculated truncated value is considerably smaller.

The fractional contribution to σ_{spc} and σ_{bspc} from the fine particles, including extinction at all angles, is 0.020 $\pm$ 0.005 and 0.0029 $\pm$ 0.0008, respectively, at a wavelength of 0.55 μm. When one repeats the procedure, having taken the angular truncation into account, the data indicate fine fractions of 0.38 $\pm$ 0.07 and 0.010 $\pm$ 0.003 for the scattering and backscattering, respectively. These can be compared with measured results in the marine boundary layer at Cape Grim, Tasmania (Carrico et al. 1998), given as 0.23 $\pm$ 0.06 for total scattering and 0.17 $\pm$ 0.06 for backscattering. Though the different datasets do not agree, the inclusion of the effects of angular truncation produces values that are much closer to those of Carrico et al. (1998). Similar results are obtained for the other two wavelengths, as summarized in Table 3.

The estimated uncertainties on all of these numbers are derived from the uncertainty in the sizing instruments. This is based upon uncertainties in the flow rate (<10%) and in the calibration of the diameter bins, given as half of the bin width divided by the midpoint diameter (approximately 10%).

c. *Analysis of hygroscopic effects*

The correction factor, as a function of relative humidity (RH), is examined in order to determine how hygroscopic effects may have contributed to the large disagreement between the calculated and measured scattering signals. The relative humidity of the ambient (outdoor) air was measured, as was the relative humidity of the nephelometer sample, which was partially dried through heating within the instrument. This sample relative humidity was recorded by a relative humidity sensor within the nephelometer. Particles sampled by the SMPS and PCASP are essentially dried, based on some degree of heating above the ambient

TABLE 3. The fine fraction of light scattering and backscattering given for calculated and calculated truncated values for all three wavelengths.

	Total scattering		Backscattering	
λ (μm)	Fine fraction of σ_{spc} (calculated)	Fine fraction of σ_{spt} (truncated)	Fine fraction of σ_{bspc} (calculated)	Fine fraction of σ_{bspt} (truncated)
0.45	0.023 ± 0.007	0.50 ± 0.07	0.007 ± 0.002	0.013 ± 0.004
0.55	0.020 ± 0.005	0.38 ± 0.07	0.0029 ± 0.0008	0.010 ± 0.003
0.70	0.010 ± 0.002	0.21 ± 0.05	0.0020 ± 0.0005	0.004 ± 0.001

temperature before the particles are detected, as well as by the drying of the sheath air by both instruments using a desiccant. Although the FSSP is a nonintrusive probe, it was located inside the same small shelter as the nephelometer. The shelter was heated relative to the ambient air by the various pumps and instruments. Thus, the sample reaching the FSSP was at a RH similar to that of the nephelometer.

Figure 13 shows the ambient relative humidity and that measured inside the nephelometer plotted with the total scattering coefficient measured by the nephelometer for green light. Some correlation between the sample RH and the total scattering coefficient is evident. If hygroscopic effects were solely responsible for the large correction factors, the more thoroughly dried samples would have a correction factor more in keeping with that of Anderson and Ogren (1998).

To test this, the data are sorted into different regimes of the sample relative humidity in the nephelometer. For each of these subsets of data a new correction factor is calculated. These results are shown in Table 4. The correction factor increases with increasing relative humidity, indicating that water very likely influenced the particle sizing, at least at relative humidities above 30%. This can also be seen in the dependence of the mean particle size measured by the FSSP on the RH (the last column of Table 4), with the increase in size resulting from the uptake of water. At relative humidities below 30%, the correction factors are still an order of magnitude above those suggested in the literature.

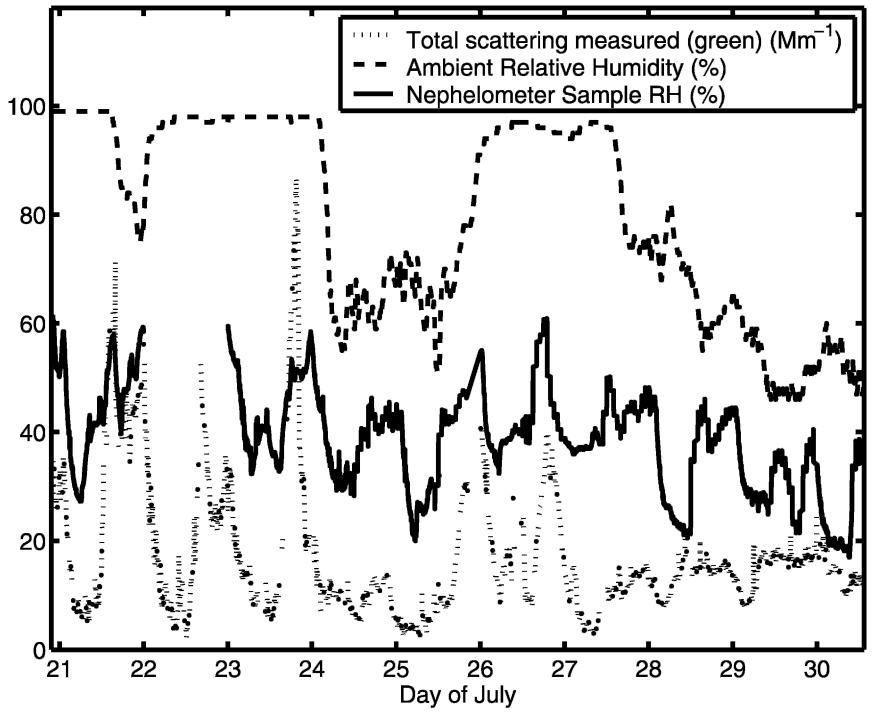

FIG. 13. The ambient relative humidity (dashed line), nephelometer-sample relative humidity (solid line), and measured scattering coefficient (dotted line) plotted together. No sample relative humidity data were collected on 22 Jul.

TABLE 4. The suggested correction factor based upon the sample relative humidity, as measured by the nephelometer.

Relative humidity range (%)	Correction factor	Hours of data in this range	Mean diameter of aerosol measured by FSSP (μm)
>60	45 ± 24	5	16.12
50–60	30 ± 10	4	11.48
40–50	24 ± 6	137	11.20
30–40	19 ± 7	141	10.51
20–30	17 ± 6	6810	9.86
<20	16 ± 1	11	9.20

The major factor influencing the number concentration of coarse marine aerosols is wind speed. The coarse particles are dominated by sea salt, and the rate of droplet production, the main source of sea salt aerosols, is a strong function of wind speed (e.g., Gong et al. 1997). The concentration of coarse particles measured by the FSSP is plotted alongside the wind speed in Fig. 14. The wind data were collected with an anemometer mounted approximately 10 m above sea level and corrected for ship speed and course over ground, after Smith et al. (1999).

Some correlation between the two can be seen, though there are a few notable exceptions, such as the spike in the FSSP numbers on the evening of 23 July, preceding the increase in wind speeds. This corresponds to a high level of sulfur species measured by the AMS, as seen in Fig. 3. The other anomalous period is from 28 to 29 July, when there are high wind speeds but low FSSP concentrations. The reason for this is unclear. Unfortunately, no wind data were recorded from the evening of 29 July onward. Throughout the cruise high wind speeds were seen, with an average speed of 7.83 m s^{-1} and a direction of 231.4° over the sampling period.

4. Discussion

The angular truncation of the nephelometer can be a very large factor when the aerosol population contains a relatively high number of coarse particles, such as in a windy marine boundary layer. In such cases, optical properties calculated from measurements of the size distribution and chemical composition are able to provide a better determination of the extinction properties than direct measurements. The difference between the measured values and those calculated using the chemical and physical measurements are striking in this case—for $\lambda = 0.55$ μm, the average measured σ_{sp} is 17

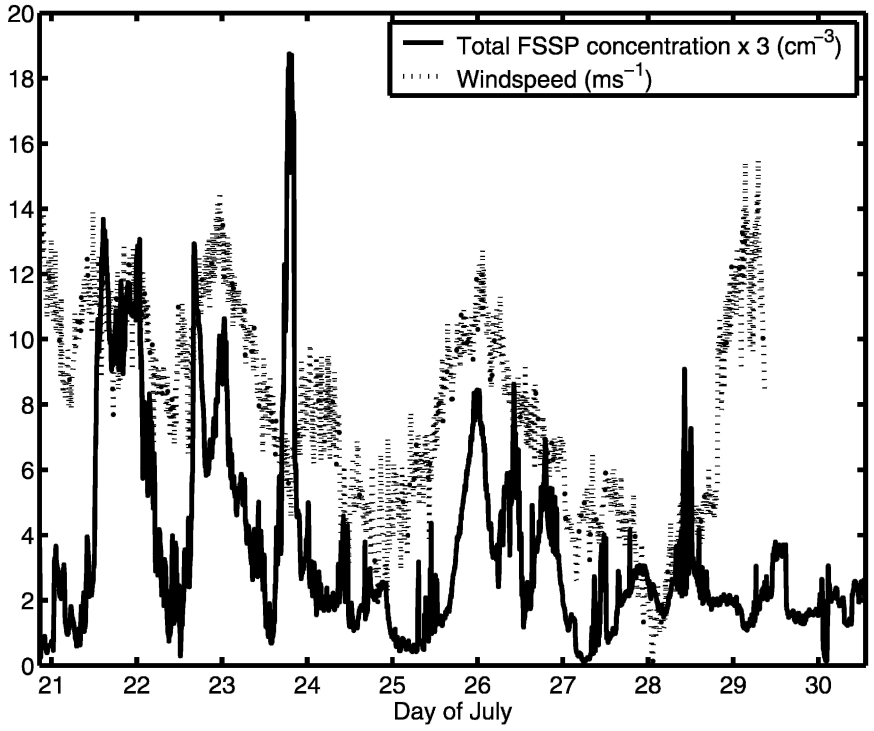

FIG. 14. The wind speed (dotted line) and 3 times the total concentration measured by the FSSP (solid line). The anemometer data were not recorded from the morning of 29 Jul to the morning of 30 Jul.

TABLE 5. Suggested correction factors for specific environments based on theoretical aerosol distributions.

Environment	Total scattering correction			Backscattering correction		
	0.45 μm	0.55 μm	0.70 μm	0.45 μm	0.55 μm	0.70 μm
Clean continental	1.34	1.34	1.36	1.30	1.28	1.28
Continental average	1.33	1.33	1.35	1.29	1.27	1.27
Continental polluted	1.30	1.30	1.31	1.27	1.25	1.25
Urban	1.31	1.31	1.33	1.26	1.25	1.25
Desert	1.94	1.75	1.60	1.62	1.58	1.53
Maritime clean	1.71	1.53	1.55	1.50	1.47	1.40
Maritime polluted	1.54	1.45	1.47	1.45	1.43	1.37
Maritime tropical	1.75	1.56	1.54	1.50	1.48	1.40
Arctic	1.36	1.33	1.35	1.35	1.34	1.30
Antarctic	1.39	1.35	1.31	1.36	1.37	1.33

$\pm$ 13 Mm^{-1}, while the average calculated σ_{spc} is 320 $\pm$ 300 Mm^{-1}. The latter value is reduced to $\sigma_{spt} = 13 \pm 7$ Mm^{-1} when the angular truncation of the nephelometer is taken into account.

The present data indicate a correction factor resulting from angular truncation far greater than that suggested in Anderson and Ogren (1998). (The correction as a result of the non-Lambertian nature of the light source was not considered here.) This is likely because of the size distribution of this particular case. The correction factor given in Anderson and Ogren (1998) is relevant for some aerosol distributions, excluding those in a windy marine boundary layer.

Table 5 gives some suggested correction factors for standard typical aerosol size distributions for a variety of environments. The aerosol size distributions are those suggested by Hess et al. (1998), with the aerosol types being water insoluble, water soluble, sea salt (accumulation mode and coarse mode), mineral dust (nucleation mode, accumulation mode, coarse mode, and transported), sulfate, and soot. The complex indices of refraction at each wavelength are taken from

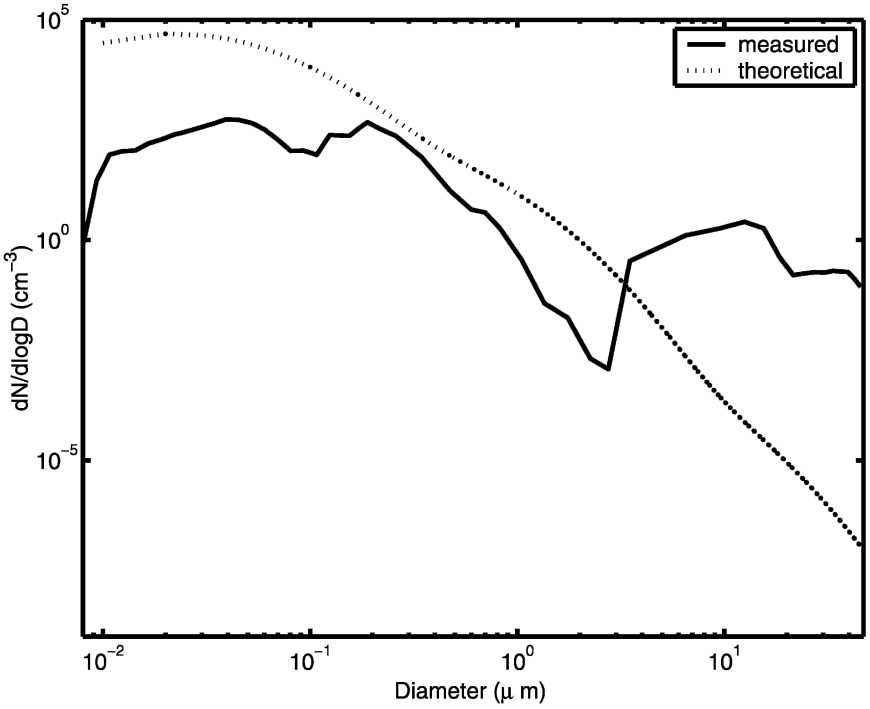

FIG. 15. The measured aerosol size distribution (solid) plotted alongside the theoretical distribution for a clean marine case (dotted). In the coarse mode the measured size distribution has a concentration over 5 times that of the theoretical distribution.

Koepke et al. (1997). The correction factors in Table 5 are similar or larger than the value suggested by Anderson and Ogren (1998). In particular, the values for the maritime cases are approximately an order of magnitude smaller than the correction factors from the present study, which most frequently has a value of 17. This is because of the fact that the number concentrations of coarse-mode particles are orders of magnitude greater than the maritime distributions of Hess et al., as illustrated in Fig. 15.

While the present results are not suggested to be representative of the global oceans on average, they indicate a potentially much greater role for sea salt in the direct effect than that suggested by theoretical distributions. The implications for high sea salt concentrations in the marine boundary layer also extend beyond the direct effect to the indirect effect of aerosols, as shown by O'Dowd et al. (1999). Over the oceans, it is not only necessary to take into account the angular truncation uncertainty in the nephelometer measurement, but also to consider a variety of meteorological conditions. One method to approach this problem was suggested by Quinn and Coffman (1998), which requires the simultaneous measurement of the size distribution and chemical composition of the aerosol to enable the calculation of a correction factor at each time step, in a similar manner as was conducted here.

5. Conclusions

The optical properties (σ_{sp}, σ_{bsp}, and σ_{abs}) of the aerosols in a remote marine area were measured over a 10-day period coincident with measurements of the aerosol particle size distribution and chemical composition. The particle size and chemical data were applied in a Mie scattering model in an effort to examine optical closure. The resulting calculated and measured extinction parameters did not compare well before considering the angular limitations of the nephelometer. Taking those limitations into account led to agreement to within 15% in most cases.

Scattering apportionment by size indicates that the vast majority of the scattering and backscattering during the SERIES cruise in the North Pacific was a result of coarse particles, with the majority attributed to particles greater than 10 μm in diameter. The large correction factor that was needed to account for the angular limitations of the nephelometer (median of approximately 17) suggests that to estimate scattering from coarse particles the best approach that is currently available may be to calculate it from independent measurements of the size distribution and chemical composition of the aerosol. New techniques (e.g., cavity ring down, Strawa et al. 2003) may provide a direct solution to this problem.

Acknowledgments. The authors thank CFCAS and NSERC for funding through the SOLAS network grant. Thanks are given to Steve Bacic and Armand Gaudenzi of the Meteorological Service of Canada for their work in installing the instruments, the captain and crew of *El Puma* for all of their assistance throughout, and Frank Whitney of the Institute of Ocean Sciences for acting as our contact on land. Thanks are also given to the three anonymous reviewers for their helpful comments and suggestions.

REFERENCES

Anderson, T. L., and J. A. Ogren, 1998: Determining aerosol radiative properties using the TSI 3563 integrating nephelometer. *Aerosol Sci. Technol.,* **29,** 57–69.

——, and Coauthors, 1996: Performance characteristics of a high-sensitivity, three-wavelength total scatter/backscatter nephelometer. *J. Atmos. Oceanic Technol.,* **13,** 967–986.

——, D. S. Covert, J. D. Wheeler, J. M. Harris, K. D. Perry, B. E. Trost, D. J. Jaffe, and J. A. Ogren, 1999: Aerosol backscatter fraction and single scattering albedo: Measured values and uncertainties at a coastal station in the pacific northwest. *J. Geophys. Res.,* **104,** 26 793–26 807.

Bohren, C. F., and D. R. Huffman, 1998: *Absorption and Scattering of Light by Small Particles.* John Wiley and Sons, 544 pp.

Bond, T. C., T. L. Anderson, and D. Campbell, 1999: Calibration and intercomparison of filter-based measurements of visible light absorption by aerosols. *Aerosol Sci. Technol.,* **30,** 582–600.

Carrico, C. M., M. J. Rood, and J. A. Ogren, 1998: Aerosol light scattering properties at Cape Grim, Tasmania, during the First Aerosol Characterization Experiment. *J. Geophys. Res.,* **103,** 16 565–16 574.

Gong, S. L., L. A. Barrie, and J. P. Blanchet, 1997: Modeling sea-salt aerosols in the atmosphere, 1. Model development. *J. Geophys. Res.,* **102,** 3805–3818.

Heintzenberg, J., R. J. Charlson, A. D. Clarke, C. Liousse, V. Ramaswamy, K. P. Shine, M. Wendisch, and G. Helas, 1997: Measurements and modelling of aerosol single-scattering albedo: Progress, problems and prospects. *Beitr. Phys. Atmos.,* **70,** 249–263.

Hess, M., P. Keopke, and I. Schult, 1998: Optical properties of aerosols and clouds: The software package OPAC. *Bull. Amer. Meteor. Soc.,* **79,** 831–834.

Koepke, P., M. Hess, I. Schult, and E. P. Shettle, 1997: Global Aerosol Data Set. MPI Meteorologie Hamburg Rep. 243, 44 pp.

Li, S., K. B. Strawbridge, W. R. Leaitch, and A. M. Macdonald, 1998: Aerosol backscattering determined from chemical and physical properties and lidar observations over the east coast of Canada. *Geophys. Res. Lett.,* **25,** 1653–1656.

Liousse, C., J. E. Penner, C. Chuang, J. J. Walton, and H. Eddleman, 1996: A global three-dimensional model study of carbonaceous aerosols. *J. Geophys. Res.,* **101,** 19 411–19 432.

O'Dowd, C. D., J. A. Lowe, and M. H. Smith, 1999: The relative importance of non-sea-salt sulphate and sea-salt aerosol to

the marine cloud condensation nuclei population: An improved multi-component aerosol-cloud droplet parameterization. *Quart. J. Roy. Meteor. Soc.,* **125,** 1311–1314.

Quinn, P. K., and D. J. Coffman, 1998: Local closure during the First Aerosol Characterization Experiment (ACE 1): Aerosol mass concentration and scattering and backscattering coefficients. *J. Geophys. Res.,* **103,** 16 575–16 596.

Seinfeld, J. H., and S. N. Pandis, 1998: *Atmospheric Chemistry and Physics.* John Wiley and Sons, 1326 pp.

Smirnov, A., Y. Villevalde, N. T. O'Neill, A. Royer, and A. Tarussov, 1995: Aerosol optical depth over the oceans: Analysis in terms of synoptic air mass types. *J. Geophys. Res.,* **100,** 16 639–16 650.

Smith, S. R., M. A. Bourassa, and R. J. Sharp, 1999: Establishing more truth in true winds. *J. Atmos. Oceanic Technol.,* **16,** 939–952.

Strawa, A. W., R. Castaneda, T. Owano, D. S. Baer, and B. A. Paldus, 2003: The measurement of aerosol optical properties using continuous wave cavity ring-down techniques. *J. Atmos. Oceanic Technol.,* **20,** 454–465.

Tang, I. N., 1996: Chemical and size effects of hygroscopic aerosols on light scattering coefficients. *J. Geophys. Res.,* **101,** 19 245–19 250.

——, 1997: Thermodynamic and optical properties of mixed-salt aerosols of atmospheric importance. *J. Geophys. Res.,* **102,** 1883–1893.

Toon, O. B., J. B. Pollack, and B. N. Khare, 1976: The optical constants of several atmospheric aerosol species: Ammonium sulfate, aluminum oxide, and sodium chloride. *J. Geophys. Res.,* **81,** 5733–5745.

Zhang, X. F., K. A. Smith, D. R. Worsnop, J. Jimenez, J. T. Jayne, and C. E. Kolb, 2002: A numerical characterization of particle beam collimation by an aerodynamic lens-nozzle system. Part 1, An individual lens or nozzle. *Aerosol Sci. Technol.,* **36,** 617–631.